Deep–Sea Research I 208 (2024) 104301

Contents lists available at ScienceDirect

Deep-Sea Research Part I

journal homepage: www.elsevier.com/locate/dsri

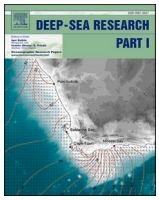

Dispersion of waves propagating in the ice-covered Arctic Ocean

Shengxing Liu [a,b,*], Qitian Zeng [a], Liguo Tang [a], Zhenglin Li [b,c,d]

[a] College of Ocean and Earth Sciences, Xiamen University, Xiamen, 361102, China
[b] Southern Marine Science and Engineering Guangdong Laboratory (Zhuhai), Zhuhai, 519000, China
[c] School of Ocean Engineering and Technology, Sun Yat-sen University, Zhuhai, 519000, China
[d] Key Laboratory of Comprehensive Observation of Polar Environment (Sun Yat-sen University), Ministry of Education, China

ARTICLE INFO

Keywords:
Arctic ocean
Acoustic propagation
Dispersion
Ice cover
Transfer matrix

ABSTRACT

The Arctic Ocean was modeled as an ice–seawater–sediment system, where the ice cover and seawater were assumed to be inhomogeneous solid and liquid, respectively, while the sediment was assumed to be homogeneous liquid. Transfer matrixes relating the displacements and stresses at the lower surface and those at the upper surface for a thin solid layer, and a thin liquid layer were derived. Furthermore, a dispersion equation for waves propagating in the ice-covered Arctic Ocean was derived using the transfer matrix technique. The phase- and group-velocity dispersion curves were obtained by solving the dispersion equation numerically. The results show that the dispersion curves for the Arctic Ocean with ice cover are much more complex than those without ice cover. Except for the new mode, the phase-velocity curve for the n-th ($n > 2$) mode exhibited a slight distortion, which caused a sharp peak in the group-velocity curve. These peak values, which depend on the order of the mode, may be significantly higher than the speed of sound in seawater. The variation of the ice cover thickness had significant influence on the dispersion curves of the first and second modes. Moreover, the influence of the seawater depth on the dispersion curves were investigated.

1. Introduction

Acoustic propagation in the ice-covered Arctic Ocean has great significance in both military and civil area. Several studies have been conducted on acoustic propagation in the Arctic Ocean in the past century. In 1959, a series of experiments (Kutschale, 1961) were performed to investigate acoustic propagation in the central Arctic Ocean, where Trinitrotoluene (TNT) was used as the explosive acoustic source and hydrophones and geophones were used to detect acoustic signals in the water and on the ice surface, respectively. In these experiments, at least two normal modes were observed at a distance of up to 1150 km from the source. The dispersion curves obtained in these experiments were in good agreement with theoretical results (Kutschale, 1961). Hunkins and Kutschale (1963) investigated the dispersion of acoustic propagation on the Arctic continental shelf, north of Alaska at short-range (between 2 and 10 km) and long-range (between 50 and 250 km) distances. Diachok (1976) investigated the influence of ice ridges on acoustic propagation in the central Arctic Ocean using the Ray theory and Burke Twersky (BT) scattering models. Lepage and Schmidt (1994) studied low-frequency transmission loss in the central Arctic using the normal model KRAKEN and perturbation theory.

In recent years, sea ice has become thinner and the ice-covered area has become smaller owing to the rapid rise in the global annual average temperature (Münchow et al., 2014; Shroyer et al., 2017; Kwok and Rothrock, 2009), which is convenient for performing human activities in the Arctic. Studying acoustic propagation in the under-ice environment is important for performing human activities in the Arctic, such as oceanographic surveys and exploration of submarine oil and gas resources (Frank and Ivakin, 2018; Freitag et al., 2015; Keen et al., 2018). Gavrilov and Mikhalevsky (2006) studied the transmission loss between the Franz Victoria Strait and the Lincoln Sea in the Arctic using data from Arctic climate observations. Hope et al. (2017) studied low-frequency acoustic propagation underneath rough Arctic sea ice using the full wave integration model, OASES. Penhale et al. (2018) performed several experiments to investigate the transmission loss of multipath propagation in the shallow Arctic Ocean. Liu et al. (2019) studied the impulse response and transmission loss in the Petermann Fjord Arctic by combining the ray model, BELLHOP, and the reflecting model. All the aforementioned studies showed that ice cover and sound speed profile are the two key factors affecting acoustic propagation in the Arctic Ocean.

The spatial distribution of ice cover in the Arctic is complex. The

* Corresponding author. College of Ocean and Earth Sciences, Xiamen University, Xiamen, 361102, China.
E-mail address: liusx@xmu.edu.cn (S. Liu).

https://doi.org/10.1016/j.dsr.2024.104301
Received 29 June 2023; Received in revised form 29 March 2024; Accepted 16 April 2024
Available online 17 April 2024

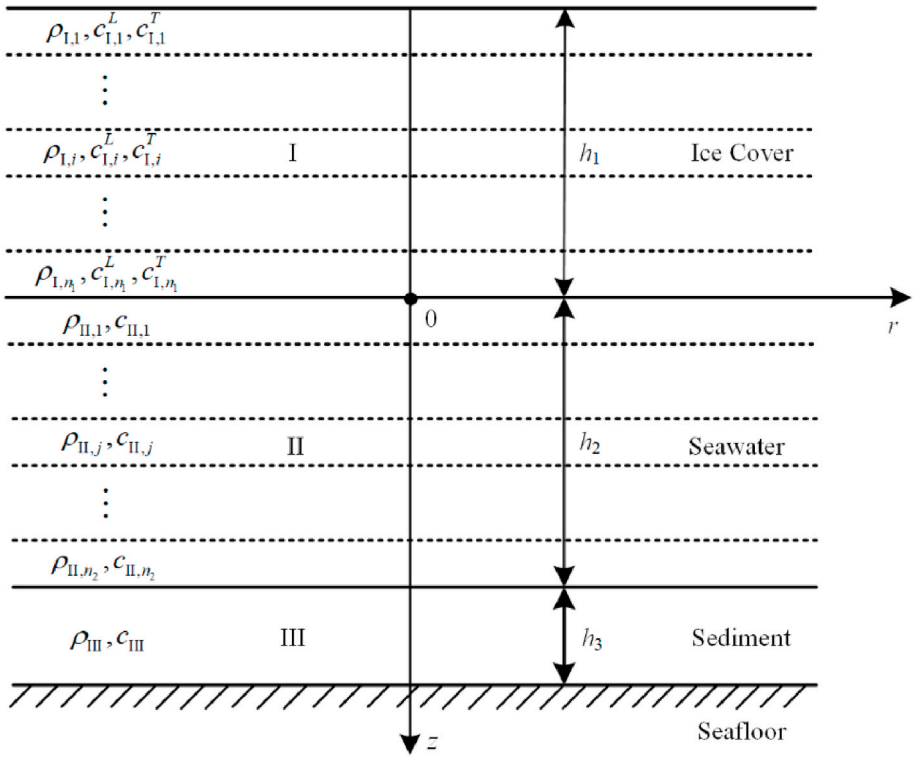

Fig. 1. Arctic Ocean acoustic model.

dimension and acoustic parameters of ice cover change with climate and season (Haas et al., 2010; Schwarz et al., 1977; Jezek et al., 1990). Generally, ice cover is thinner in summer than it is in winter. One-year-new ice covers are loose and high in salt content, but multi-year-old ice covers are hard and brittle. Ice covers are composed of different layers of ice from various years, exhibiting stratified distribution. These layers have different densities and elastic constants. The elastic medium (McCammon and Mcdamoel, 1985) and ice ridge models (Burke and Twersky, 1966) are often used to study the effect of ice cover on acoustic propagation. The former focuses on the effects of thickness and acoustic parameters of ice cover on acoustic propagation, whereas the latter focuses on the effect of ice ridges. The Arctic Ocean has a typical positive sound velocity gradient, which causes the acoustic waves to refract upward (Mikhalevsky et al., 1999).

The normal model is one of the most popular methods used to simulate underwater low-frequency acoustic propagation owing to its clear physical concept, accurate result, and high computation efficiency. Although there are many published works on the application of the normal model for open waters (Porter and Reiss, 1984; Porter and Reiss, 1985; Boyles, 1983), most of them are not applicable to the Arctic Ocean with ice cover. Therefore, to analyze acoustic propagation in the Arctic Ocean (Keen et al., 2018; Collis et al., 2016), it is necessary to develop an under-ice normal model. In this study, the Arctic Ocean was assumed to be an ice (solid)–seawater (liquid)–sediment (liquid) system, where the ice cover and seawater were divided into n_1 and n_2 thin homogeneous layers, respectively. Then, the dispersion equation for waves propagating in the ice-covered Arctic Ocean was derived using the transfer matrix technique. Moreover, the phase- and group-velocity dispersion curves were obtained by solving the dispersion equation numerically. The influence of ice cover on dispersion was analyzed based on the dispersion curves corresponding to the waves in the Arctic Ocean with and without ice cover. Compared with the method presented by Kutschale (1961), the method presented herein is applicable to the Arctic Ocean with depth-varying sound speed and density. Moreover, it can be used to study high-frequency acoustic-wave propagation in deep water.

2. Arctic Ocean acoustic model

The Arctic Ocean acoustic model is shown in Fig. 1. Media I, II, and III are ice cover, seawater, and sediment, respectively. Their thicknesses are h_1, h_2, and h_3, respectively. To simplify the model, the ice cover is assumed to be an elastic solid. Its density, longitudinal and transverse wave velocities are $\rho_I(z)$, $c_I^L(z)$ and $c_I^T(z)$, respectively. The density and sound velocity corresponding to seawater are $\rho_{II}(z)$ and $c_{II}(z)$, respectively. The sediment is assumed to be a homogeneous liquid layer supporting only longitudinal waves (Jensen et al., 2011; He et al., 2023). Its density and sound velocity are ρ_{III} and c_{III}, respectively. The upper surface of the ice cover is free, whereas the lower surface of the sediment is rigid. A cylindrical coordinate system is used in this study. Its origin is located at the interface between media I and II, whereas its r and z axes are parallel and normal to the interface, respectively. Only axisymmetric waves propagating along the r direction were considered in this study.

Ice cover is divided into n_1 layers for the purpose of convenient deriving. The thickness of each thin ice layer is $\Delta h_1 = h_1/n_1$. When Δh_1 is small enough, each thin ice layer can be assumed to be homogeneous. The density, longitudinal and transverse wave velocities corresponding to the i-th thin ice layer are $\rho_{I,i}$, $c^L_{I,i}$ and $c^T_{I,i}$ ($i = 1, 2, \ldots, n_1$), respectively. Similarly, Seawater is divided into n_2 thin layers, and the thickness of each seawater layer is $\Delta h_2 = h_2/n_2$. The density and sound velocity corresponding to the j-th seawater layer are $\rho_{II,j}$ and $c_{II,j}$ (j=1, 2, …, n_2), respectively.

3. Theory

3.1. Displacement and stress

In Fig. 1, assuming that the displacement potential functions corresponding to the longitudinal and transverse waves in the i-th (i=1, 2, …, n_1) thin ice layer are $\varphi_{I,i}$ and $\chi_{I,i}$, respectively, and those corresponding to the j-th (j=1, 2, …, n_2) thin seawater layer and the sediment are $\varphi_{II,j}$ and φ_{III}, respectively, we have

$$\varphi_{\mathrm{I},i} = \left(A_{\mathrm{I},i}\cos\alpha_{\mathrm{I},i}z + B_{\mathrm{I},i}\sin\alpha_{\mathrm{I},i}z\right)J_0(\xi r), \tag{1}$$

$$\chi_{\mathrm{I},i} = \left(C_{\mathrm{I},i}\cos\beta_{\mathrm{I},i}z + D_{\mathrm{I},i}\sin\beta_{\mathrm{I},i}z\right)J_0(\xi r), \tag{2}$$

$$\varphi_{\mathrm{II},j} = \left(A_{\mathrm{II},j}\cos\alpha_{\mathrm{II},j}z + B_{\mathrm{II},j}\sin\alpha_{\mathrm{II},j}z\right)J_0(\xi r), \tag{3}$$

and

$$\varphi_{\mathrm{III}} = \left(A_{\mathrm{III}}\cos\alpha_{\mathrm{III}}z + B_{\mathrm{III}}\sin\alpha_{\mathrm{III}}z\right)J_0(\xi r), \tag{4}$$

where $\alpha_{\mathrm{I},i} = \sqrt{(\omega/c_{\mathrm{I},i}^{L})^2 - \xi^2}$, $\beta_{\mathrm{I},i} = \sqrt{(\omega/c_{\mathrm{I},i}^{T})^2 - \xi^2}$, $\alpha_{\mathrm{II},j} = \sqrt{(\omega/c_{\mathrm{II},j})^2 - \xi^2}$, $\alpha_{\mathrm{III}} = \sqrt{(\omega/c_{\mathrm{III}})^2 - \xi^2}$, ξ is the wavenumber along r direction, ω is the angular frequency, $A_{\mathrm{I},i}$, $B_{\mathrm{I},i}$, $C_{\mathrm{I},i}$, $D_{\mathrm{I},i}$ (i=1, 2, …, n_1), $A_{\mathrm{II},j}$, $B_{\mathrm{II},j}$ (j=1, 2, …, n_2), A_{III}, and B_{III} are the constants to be determined, and $J_0(\cdot)$ is the first kind of Bessel function of order zero. The time variable $e^{j\omega t}$ is omitted from Eqs (1)–(4) and the succeeding equations.

According to the relationship between displacement, stress, and displacement potential function (Eringen and Suhubi, 1975), the displacements $u_{\mathrm{I},i}^{z}$ and $u_{\mathrm{I},i}^{r}$ and stress $\sigma_{\mathrm{I},i}^{zz}$ and $\sigma_{\mathrm{I},i}^{rz}$ corresponding to the i-th (i=1, 2, …, n_1) thin ice layer are described as

$$u_{\mathrm{I},i}^{z} = \left[\alpha_{\mathrm{I},i}\left(-A_{\mathrm{I},i}\sin\alpha_{\mathrm{I},i}z + B_{\mathrm{I},i}\cos\alpha_{\mathrm{I},i}z\right) + \xi^2\left(C_{\mathrm{I},i}\cos\beta_{\mathrm{I},i}z + D_{\mathrm{I},i}\sin\beta_{\mathrm{I},i}z\right)\right]J_0(\xi r), \tag{5}$$

$$u_{\mathrm{I},i}^{r} = \xi\left[\left(A_{\mathrm{I},i}\cos\alpha_{\mathrm{I},i}z + B_{\mathrm{I},i}\sin\alpha_{\mathrm{I},i}z\right) + \beta_{\mathrm{I},i}\left(-C_{\mathrm{I},i}\sin\beta_{\mathrm{I},i}z + D_{\mathrm{I},i}\cos\beta_{\mathrm{I},i}z\right)\right]J_0'(\xi r), \tag{6}$$

$$\sigma_{\mathrm{I},i}^{zz} = \mu_{\mathrm{I},i}\left[\left(\xi^2 - \beta_{\mathrm{I},i}^2\right)\left(A_{\mathrm{I},i}\cos\alpha_{\mathrm{I},i}z + B_{\mathrm{I},i}\sin\alpha_{\mathrm{I},i}z\right) + 2\xi^2\beta_{\mathrm{I},i}\left(-C_{\mathrm{I},i}\sin\beta_{\mathrm{I},i}z + D_{\mathrm{I},i}\cos\beta_{\mathrm{I},i}z\right)\right]J_0(\xi r), \tag{7}$$

and

$$\sigma_{\mathrm{I},i}^{rz} = \mu_{\mathrm{I},i}\xi\left[2\alpha_{\mathrm{I},i}\left(-A_{\mathrm{I},i}\sin\alpha_{\mathrm{I},i}z + B_{\mathrm{I},i}\cos\alpha_{\mathrm{I},i}z\right) + \left(\xi^2 - \beta_{\mathrm{I},i}^2\right)\left(C_{\mathrm{I},i}\cos\beta_{\mathrm{I},i}z + D_{\mathrm{I},i}\sin\beta_{\mathrm{I},i}z\right)\right]J_0'(\xi r), \tag{8}$$

where $\mu_{\mathrm{I},i} = \rho_{\mathrm{I},i}(c_{\mathrm{I},i}^{T})^2$ is the second Lame constants of the i-th thin ice layer. The normal displacement $u_{\mathrm{II},j}^{z}$ and normal stress $\sigma_{\mathrm{II},j}^{zz}$ corresponding to the j-th thin seawater layer are described as

$$u_{\mathrm{II},j}^{z} = \alpha_{\mathrm{II},j}\left(-A_{\mathrm{II},j}\sin\alpha_{\mathrm{II},j}z + B_{\mathrm{II},j}\cos\alpha_{\mathrm{II},j}z\right)J_0(\xi r), \tag{9}$$

and

$$\sigma_{\mathrm{II},j}^{zz} = -\rho_{\mathrm{II},j}\omega^2\left(A_{\mathrm{II},j}\cos\alpha_{\mathrm{II},j}z + B_{\mathrm{II},j}\sin\alpha_{\mathrm{II},j}z\right)J_0(\xi r). \tag{10}$$

The normal displacement u_{III}^{z} and normal stress $\sigma_{\mathrm{III}}^{zz}$ corresponding to the sediment are described as

$$u_{\mathrm{III}}^{z} = \alpha_{\mathrm{III}}\left(-A_{\mathrm{III}}\sin\alpha_{\mathrm{III}}z + B_{\mathrm{III}}\cos\alpha_{\mathrm{III}}z\right)J_0(\xi r), \tag{11}$$

and

$$\sigma_{\mathrm{III}}^{zz} = -\rho_{\mathrm{III}}\omega^2\left(A_{\mathrm{III}}\cos\alpha_{\mathrm{III}}z + B_{\mathrm{III}}\sin\alpha_{\mathrm{III}}z\right)J_0(\xi r). \tag{12}$$

3.2. Transfer matrix

3.2.1. Transfer matrix of a thin ice layer

Assuming the upper and the lower surfaces of the i-th (i=1, 2, …, n_1) thin ice layer are located at h_i' and $h_{i+1}' = h_i' + \Delta h_1$, respectively. According to Eqs. (5)–(8), the displacements and stresses at the lower surface of the i-th ice thin layer are given by

$$\left.\begin{bmatrix} u_{\mathrm{I},i}^{z} \\ u_{\mathrm{I},i}^{r} \\ \sigma_{\mathrm{I},i}^{zz} \\ \sigma_{\mathrm{I},i}^{rz} \end{bmatrix}\right|_{z=h_{i+1}} = \begin{bmatrix} -\alpha_{\mathrm{I},i}\sin(\alpha_{\mathrm{I},i}h_{i+1})J_0(\xi r) & \alpha_{\mathrm{I},i}\cos(\alpha_{\mathrm{I},i}h_{i+1})J_0(\xi r) & \xi^2\cos(\beta_{\mathrm{I},i}h_{i+1})J_0(\xi r) & \xi^2\sin(\beta_{\mathrm{I},i}h_{i+1})J_0(\xi r) \\ \xi\cos(\alpha_{\mathrm{I},i}h_{i+1})J_0'(\xi r) & \xi\sin(\alpha_{\mathrm{I},i}h_{i+1})J_0'(\xi r) & -\xi\beta_{\mathrm{I},i}\sin(\beta_{\mathrm{I},i}h_{i+1})J_0'(\xi r) & \xi\beta_{\mathrm{I},i}\cos(\beta_{\mathrm{I},i}h_{i+1})J_0'(\xi r) \\ \mu_{\mathrm{I},i}\left(\xi^2-\beta_{\mathrm{I},i}^2\right)\cos(\alpha_{\mathrm{I},i}h_{i+1})J_0(\xi r) & \mu_{\mathrm{I},i}\left(\xi^2-\beta_{\mathrm{I},i}^2\right)\sin(\alpha_{\mathrm{I},i}h_{i+1})J_0(\xi r) & -2\mu_{\mathrm{I},i}\xi^2\beta_{\mathrm{I},i}\sin(\beta_{\mathrm{I},i}h_{i+1})J_0(\xi r) & 2\mu_{\mathrm{I},i}\xi^2\beta_{\mathrm{I},i}\cos(\beta_{\mathrm{I},i}h_{i+1})J_0(\xi r) \\ -2\mu_{\mathrm{I},i}\alpha_{\mathrm{I},i}\xi\sin(\alpha_{\mathrm{I},i}h_{i+1})J_0'(\xi r) & 2\mu_{\mathrm{I},i}\alpha_{\mathrm{I},i}\xi\cos(\alpha_{\mathrm{I},i}h_{i+1})J_0'(\xi r) & \mu_{\mathrm{I},i}\xi\left(\xi^2-\beta_{\mathrm{I},i}^2\right)\cos(\beta_{\mathrm{I},i}h_{i+1})J_0'(\xi r) & \mu_{\mathrm{I},i}\xi\left(\xi^2-\beta_{\mathrm{I},i}^2\right)\sin(\beta_{\mathrm{I},i}h_{i+1})J_0'(\xi r) \end{bmatrix}\begin{bmatrix} A_{\mathrm{I},i} \\ B_{\mathrm{I},i} \\ C_{\mathrm{I},i} \\ D_{\mathrm{I},i} \end{bmatrix}, \tag{13}$$

and the displacements and stresses at the upper surface of the i-th ice thin layer are given by

$$\left.\begin{bmatrix} u_{\mathrm{I},i}^{z} \\ u_{\mathrm{I},i}^{r} \\ \sigma_{\mathrm{I},i}^{zz} \\ \sigma_{\mathrm{I},i}^{rz} \end{bmatrix}\right|_{z=h_i} = \begin{bmatrix} -\alpha_{\mathrm{I},i}\sin(\alpha_{\mathrm{I},i}h_i)J_0(\xi r) & \alpha_{\mathrm{I},i}\cos(\alpha_{\mathrm{I},i}h_i)J_0(\xi r) & \xi^2\cos(\beta_{\mathrm{I},i}h_i)J_0(\xi r) & \xi^2\sin(\beta_{\mathrm{I},i}h_i)J_0(\xi r) \\ \xi\cos(\alpha_{\mathrm{I},i}h_i)J_0'(\xi r) & \xi\sin(\alpha_{\mathrm{I},i}h_i)J_0'(\xi r) & -\xi\beta_{\mathrm{I},i}\sin(\beta_{\mathrm{I},i}h_i)J_0'(\xi r) & \xi\beta_{\mathrm{I},i}\cos(\beta_{\mathrm{I},i}h_i)J_0'(\xi r) \\ \mu_{\mathrm{I},i}\left(\xi^2-\beta_{\mathrm{I},i}^2\right)\cos(\alpha_{\mathrm{I},i}h_i)J_0(\xi r) & \mu_{\mathrm{I},i}\left(\xi^2-\beta_{\mathrm{I},i}^2\right)\sin(\alpha_{\mathrm{I},i}h_i)J_0(\xi r) & -2\mu_{\mathrm{I},i}\xi^2\beta_{\mathrm{I},i}\sin(\beta_{\mathrm{I},i}h_i)J_0(\xi r) & 2\mu_{\mathrm{I},i}\xi^2\beta_{\mathrm{I},i}\cos(\beta_{\mathrm{I},i}h_i)J_0(\xi r) \\ -2\mu_{\mathrm{I},i}\alpha_{\mathrm{I},i}\xi\sin(\alpha_{\mathrm{I},i}h_i)J_0'(\xi r) & 2\mu_{\mathrm{I},i}\alpha_{\mathrm{I},i}\xi\cos(\alpha_{\mathrm{I},i}h_i)J_0'(\xi r) & \mu_{\mathrm{I},i}\xi\left(\xi^2-\beta_{\mathrm{I},i}^2\right)\cos(\beta_{\mathrm{I},i}h_i)J_0'(\xi r) & \mu_{\mathrm{I},i}\xi\left(\xi^2-\beta_{\mathrm{I},i}^2\right)\sin(\beta_{\mathrm{I},i}h_i)J_0'(\xi r) \end{bmatrix}\begin{bmatrix} A_{\mathrm{I},i} \\ B_{\mathrm{I},i} \\ C_{\mathrm{I},i} \\ D_{\mathrm{I},i} \end{bmatrix}, \tag{14}$$

Eliminating constants $A_{\mathrm{I},i}$, $B_{\mathrm{I},i}$, $C_{\mathrm{I},i}$ and $D_{\mathrm{I},i}$ in Eqs. (13) and (14), we obtain

$$\mathbf{U}_{\mathrm{I},i}\big|_{z=h_{i+1}} = \mathbf{M}_{\mathrm{I},i}\mathbf{U}_{\mathrm{I},i}\big|_{z=h_i}, \tag{15}$$

where $\mathbf{U}_{\mathrm{I},i} = [u_{\mathrm{I},i}^{z}, u_{\mathrm{I},i}^{r}, \sigma_{\mathrm{I},i}^{zz}, \sigma_{\mathrm{I},i}^{rz}]^{\mathrm{T}}$, superscript "T" indicates transposing; $\mathbf{M}_{\mathrm{I},i}$ is the transfer matrix corresponding to the i-th thin ice layer. $\mathbf{M}_{\mathrm{I},i}$ is given by

$$\mathbf{M}_{\mathrm{I},i}=\begin{bmatrix} -\alpha_{\mathrm{I},i}\sin(\alpha_{\mathrm{I},i}h_{i+1})J_0(\xi r) & \alpha_{\mathrm{I},i}\cos(\alpha_{\mathrm{I},i}h_{i+1})J_0(\xi r) & \xi^2\cos(\beta_{\mathrm{I},i}h_{i+1})J_0(\xi r) & \xi^2\sin(\beta_{\mathrm{I},i}h_{i+1})J_0(\xi r) \\ \xi\cos(\alpha_{\mathrm{I},i}h_{i+1})J_0'(\xi r) & \xi\sin(\alpha_{\mathrm{I},i}h_{i+1})J_0'(\xi r) & -\xi\beta_{\mathrm{I},i}\sin(\beta_{\mathrm{I},i}h_{i+1})J_0'(\xi r) & \xi\beta_{\mathrm{I},i}\cos(\beta_{\mathrm{I},i}h_{i+1})J_0'(\xi r) \\ \mu_{\mathrm{I},i}\left(\xi^2-\beta_{\mathrm{I},i}^2\right)\cos(\alpha_{\mathrm{I},i}h_{i+1})J_0(\xi r) & \mu_{\mathrm{I},i}\left(\xi^2-\beta_{\mathrm{I},i}^2\right)\sin(\alpha_{\mathrm{I},i}h_{i+1})J_0(\xi r) & -2\mu_{\mathrm{I},i}\xi^2\beta_{\mathrm{I},i}\sin(\beta_{\mathrm{I},i}h_{i+1})J_0(\xi r) & 2\mu_{\mathrm{I},i}\xi^2\beta_{\mathrm{I},i}\cos(\beta_{\mathrm{I},i}h_{i+1})J_0(\xi r) \\ -2\mu_{\mathrm{I},i}\alpha_{\mathrm{I},i}\xi\sin(\alpha_{\mathrm{I},i}h_{i+1})J_0'(\xi r) & 2\mu_{\mathrm{I},i}\alpha_{\mathrm{I},i}\xi\cos(\alpha_{\mathrm{I},i}h_{i+1})J_0'(\xi r) & \mu_{\mathrm{I},i}\xi\left(\xi^2-\beta_{\mathrm{I},i}^2\right)\cos(\beta_{\mathrm{I},i}h_{i+1})J_0'(\xi r) & \mu_{\mathrm{I},i}\xi\left(\xi^2-\beta_{\mathrm{I},i}^2\right)\sin(\beta_{\mathrm{I},i}h_{i+1})J_0'(\xi r) \end{bmatrix},$$
$$\begin{bmatrix} -\alpha_{\mathrm{I},i}\sin(\alpha_{\mathrm{I},i}h_i)J_0(\xi r) & \alpha_{\mathrm{I},i}\cos(\alpha_{\mathrm{I},i}h_i)J_0(\xi r) & \xi^2\cos(\beta_{\mathrm{I},i}h_i)J_0(\xi r) & \xi^2\sin(\beta_{\mathrm{I},i}h_i)J_0(\xi r) \\ \xi\cos(\alpha_{\mathrm{I},i}h_i)J_0'(\xi r) & \xi\sin(\alpha_{\mathrm{I},i}h_i)J_0'(\xi r) & -\xi\beta_{\mathrm{I},i}\sin(\beta_{\mathrm{I},i}h_i)J_0'(\xi r) & \xi\beta_{\mathrm{I},i}\cos(\beta_{\mathrm{I},i}h_i)J_0'(\xi r) \\ \mu_{\mathrm{I},i}\left(\xi^2-\beta_{\mathrm{I},i}^2\right)\cos(\alpha_{\mathrm{I},i}h_i)J_0(\xi r) & \mu_{\mathrm{I},i}\left(\xi^2-\beta_{\mathrm{I},i}^2\right)\sin(\alpha_{\mathrm{I},i}h_i)J_0(\xi r) & -2\mu_{\mathrm{I},i}\xi^2\beta_{\mathrm{I},i}\sin(\beta_{\mathrm{I},i}h_i)J_0(\xi r) & 2\mu_{\mathrm{I},i}\xi^2\beta_{\mathrm{I},i}\cos(\beta_{\mathrm{I},i}h_i)J_0(\xi r) \\ -2\mu_{\mathrm{I},i}\alpha_{\mathrm{I},i}\xi\sin(\alpha_{\mathrm{I},i}h_i)J_0'(\xi r) & 2\mu_{\mathrm{I},i}\alpha_{\mathrm{I},i}\xi\cos(\alpha_{\mathrm{I},i}h_i)J_0'(\xi r) & \mu_{\mathrm{I},i}\xi\left(\xi^2-\beta_{\mathrm{I},i}^2\right)\cos(\beta_{\mathrm{I},i}h_i)J_0'(\xi r) & \mu_{\mathrm{I},i}\xi\left(\xi^2-\beta_{\mathrm{I},i}^2\right)\sin(\beta_{\mathrm{I},i}h_i)J_0'(\xi r) \end{bmatrix}^{-1}, \tag{16}$$

where superscript "-1" indicates inversing. The elements of $\mathbf{M}_{\mathrm{I},i}$, which are given in Appendix A, can be obtained through simplifying Equation (16).

3.2.2. Transfer matrix of a thin seawater layer

The upper and lower surfaces of the j-th (j=1, 2, …, n_2) seawater thin layer are located at (j-1)Δh_2 and $j\Delta h_2$, respectively, as shown in Fig. 1. According to Eqs. (9) and (10), the normal displacement and normal stress at the lower surface of the j-th seawater thin layer are given by

$$\begin{bmatrix} u_{\mathrm{II},j}^z \\ T_{\mathrm{II},j}^{cz} \end{bmatrix}_{z=j\Delta h_2}=\begin{bmatrix} -\alpha_{\mathrm{II},j}\sin(\alpha_{\mathrm{II},j}j\Delta h_2) & \alpha_{\mathrm{II},j}\cos(\alpha_{\mathrm{II},j}j\Delta h_2) \\ -\rho_{\mathrm{II},j}\omega^2\cos(\alpha_{\mathrm{II},j}j\Delta h_2) & -\rho_{\mathrm{II},j}\omega^2\sin(\alpha_{\mathrm{II},j}j\Delta h_2) \end{bmatrix}\begin{bmatrix} A_{\mathrm{II},j} \\ B_{\mathrm{II},j} \end{bmatrix}. \tag{17}$$

Similarly, the normal displacement and normal stress at the upper surface of the j-th seawater thin layer are given by

$$\begin{bmatrix} u_{\mathrm{II},j}^z \\ T_{\mathrm{II},j}^{cz} \end{bmatrix}_{z=(j-1)\Delta h_2}=\begin{bmatrix} -\alpha_{\mathrm{II},j}\sin[\alpha_{\mathrm{II},j}(j-1)\Delta h_2] & \alpha_{\mathrm{II},j}\cos[\alpha_{\mathrm{II},j}(j-1)\Delta h_2] \\ -\rho_{\mathrm{II},j}\omega^2\cos[\alpha_{\mathrm{II},j}(j-1)\Delta h_2] & -\rho_{\mathrm{II},j}\omega^2\sin[\alpha_{\mathrm{II},j}(j-1)\Delta h_2] \end{bmatrix}\begin{bmatrix} A_{\mathrm{II},j} \\ B_{\mathrm{II},j} \end{bmatrix}. \tag{18}$$

Eliminating constants $A_{\mathrm{II},k}$ and $B_{\mathrm{II},k}$ in Eqs. (17) and (18), we obtain

$$\mathbf{U}_{\mathrm{II},j}\big|_{z=j\Delta h_2}=\mathbf{M}_{\mathrm{II},j}\mathbf{U}_{\mathrm{II},j}\big|_{z=(j-1)\Delta h_2}, \tag{19}$$

where $\mathbf{U}_{\mathrm{II},j}=[u_{\mathrm{II},j}^z,\sigma_{\mathrm{II},j}^{zz}]^{\mathrm{T}}$, $\mathbf{M}_{\mathrm{II},j}$ is the transfer matrix corresponding to the j-th thin seawater layer whose elements are given by

$$(M_{\mathrm{II},j})_{11}=(M_{\mathrm{II},j})_{22}=\cos(\alpha_{\mathrm{II},j}\Delta h_2), \tag{20}$$

$$(M_{\mathrm{II},j})_{12}=\frac{\alpha_{\mathrm{II},j}\sin(\alpha_{\mathrm{II},j}\Delta h_2)}{\rho_{\mathrm{II},j}\omega^2}, \tag{21}$$

and

$$(M_{\mathrm{II},j})_{21}=-\frac{\rho_{\mathrm{II}}\omega^2\sin(\alpha_{\mathrm{II},j}\Delta h_2)}{\alpha_{\mathrm{II},j}}. \tag{22}$$

Similarly, the relationship between the normal displacement and normal stress at the lower surface and those at the upper surface of the sediment is given by

$$\mathbf{U}_{\mathrm{III}}\big|_{z=h_2+h_3}=\mathbf{M}_{\mathrm{III}}\mathbf{U}_{\mathrm{III}}\big|_{z=h_2}, \tag{23}$$

where $\mathbf{U}_{\mathrm{III}}=[u_{\mathrm{III}}^z,\sigma_{\mathrm{III}}^{zz}]^{\mathrm{T}}$, $\mathbf{M}_{\mathrm{III}}$ is the transfer matrix corresponding to the sediment whose elements can be obtained by replacing $\alpha_{\mathrm{II},j}$, $\rho_{\mathrm{II},j}$ and Δh_2 in Eqs. (20)–(22) with α_{III}, ρ_{III} and h_3, respectively.

3.3. Dispersion equation

The top surface of ice cover is free, so the following equations can be obtained:

$$\begin{cases} \sigma_{\mathrm{I},1}^{zz}\big|_{z=-h_1}=0 \\ \sigma_{\mathrm{I},1}^{rz}\big|_{z=-h_1}=0 \end{cases}. \tag{24}$$

The interface between the i-th and (i+1)-th $(i=1,2,\cdots,n_1-1)$ thin ice layers satisfies

$$\begin{cases} u_{\mathrm{I},i}^z\big|_{z=-h_1+i\Delta h_1}=u_{\mathrm{I},i+1}^z\big|_{z=-h_1+i\Delta h_1} \\ u_{\mathrm{I},i}^r\big|_{z=-h_1+i\Delta h_1}=u_{\mathrm{I},i+1}^r\big|_{z=-h_1+i\Delta h_1} \\ \sigma_{\mathrm{I},i}^{zz}\big|_{z=-h_1+i\Delta h_1}=\sigma_{\mathrm{I},i+1}^{zz}\big|_{z=-h_1+i\Delta h_1} \\ \sigma_{\mathrm{I},i}^{rz}\big|_{z=-h_1+i\Delta h_1}=\sigma_{\mathrm{I},i+1}^{rz}\big|_{z=-h_1+i\Delta h_1} \end{cases}. \tag{25}$$

The ice-water interface satisfies

$$\begin{cases} u_{\mathrm{I},n_1}^z\big|_{z=0}=u_{\mathrm{II},1}^z\big|_{z=0} \\ \sigma_{\mathrm{I},n_1}^{zz}\big|_{z=0}=\sigma_{\mathrm{II},1}^{zz}\big|_{z=0} \\ \sigma_{\mathrm{I},n_1}^{rz}\big|_{z=0}=0 \end{cases}. \tag{26}$$

The interface between j-th and (j+1)-th $(j=1,2,\cdots,n_2-1)$ thin seawater layers satisfies

$$\begin{cases} u_{\mathrm{II},j}^z\big|_{z=j\Delta h_2}=u_{\mathrm{II},j+1}^z\big|_{z=j\Delta h_2} \\ \sigma_{\mathrm{II},j}^{zz}\big|_{z=j\Delta h_2}=\sigma_{\mathrm{II},j}^{zz}\big|_{z=j\Delta h_2} \end{cases}. \tag{27}$$

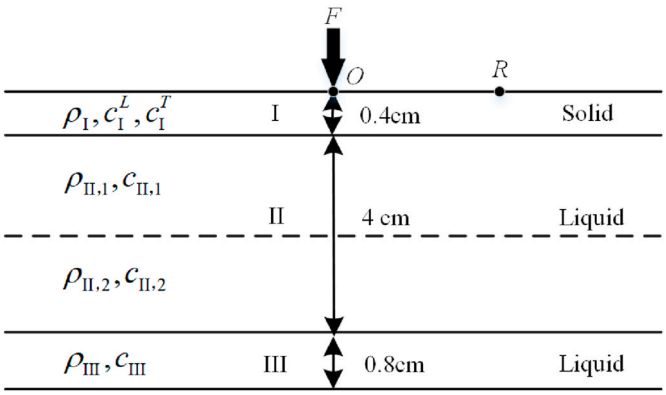

Fig. 2. Small three-layered solid-liquid-liquid structure.

The water-sediment interface satisfies

$$\begin{cases} u_{\mathrm{II},n_2}^{z}\big|_{z=h_2} = u_{\mathrm{III}}^{z}\big|_{z=h_2} \\ \sigma_{\mathrm{II},n_2}^{zz}\big|_{z=h_2} = \sigma_{\mathrm{III}}^{zz}\big|_{z=h_2} \end{cases}. \tag{28}$$

The bottom surface of the sediment satisfies

$$u_{\mathrm{III}}^{z}\big|_{z=h_2+h_3} = 0. \tag{29}$$

The displacements and the stresses at the lower surface of the n_1-th thin ice layer can be expressed by the displacements and the stresses at the upper surface of the first thin ice layer through Eqs. (15) and (25), i.e.,

$$\mathbf{U}_{\mathrm{I},n_1}\big|_{z=0} = \mathbf{M}_{\mathrm{I},n_1}\mathbf{M}_{\mathrm{I},n_1-1}\cdots\mathbf{M}_{\mathrm{I},1}\mathbf{U}_{\mathrm{I},1}\big|_{z=-h_1} = \mathbf{M}_{\mathrm{I}}\mathbf{U}_{\mathrm{I},1}\big|_{z=-h_1}. \tag{30}$$

The normal displacement and normal stress at the lower surface of the sediment can be expressed by the normal displacement and normal stress at the upper surface of the 1st thin seawater layer through Eqs. (19) and (23) and Eqs. (27) and (28), i.e.,

$$\mathbf{U}_{\mathrm{III}}\big|_{z=h_2+h_3} = \mathbf{M}_{\mathrm{III}}\mathbf{M}_{\mathrm{II},n_2}\mathbf{M}_{\mathrm{II},n_2-1}\cdots\mathbf{M}_{\mathrm{II},1}\mathbf{U}_{\mathrm{II},1}\big|_{z=0} = \mathbf{M}_{\mathrm{II}}\mathbf{U}_{\mathrm{II},1}\big|_{z=0}. \tag{31}$$

Setting i=1 in Eqs. (7)–(8) and substituting them into Eq. (24), setting i=n_1 in Eq. (5) and Eqs. (7)and (8), setting j=1 in Eqs. (9)and (10) and substituting them into Eq. (26), substituting Eq. (11) into Eq. (31), and making use of Eqs. (30)–(31), we can obtain the following equation

$$\mathbf{MA} = \mathbf{0}, \tag{32}$$

where $\mathbf{A} = [A_{\mathrm{I},1}, B_{\mathrm{I},1}, C_{\mathrm{I},1}, D_{\mathrm{I},1}, A_{\mathrm{III}}, B_{\mathrm{III}}]^{\mathrm{T}}$, $\mathbf{M}$ is a 6×6 matrix whose elements are given in Appendix B. The determinant corresponding to the matrix $\mathbf{M}$ must be zero, i.e.,

$$f(\omega,\xi) = |\mathbf{M}| = 0 \tag{33}$$

for the constants $A_{\mathrm{I},1}, B_{\mathrm{I},1}, C_{\mathrm{I},1}, D_{\mathrm{I},1}, A_{\mathrm{III},1}$, and $B_{\mathrm{III},1}$ to have nonzero solutions. This is the dispersion equation for waves propagating in the Arctic Ocean with ice cover.

4. Numerical results

4.1. Algorithm introduction

The dispersion curves for waves propagating in the Arctic Ocean with ice cover were obtained by numerically solving the dispersion equation (i.e., Eq. (33)). First, the $\omega-\xi$ dispersion curves were obtained using the bisection method. Then, the phase- and group-velocity dispersion curves were obtained using $c_p = \omega/\xi$ and $c_g = \mathrm{d}\omega/\mathrm{d}\xi$, where c_p and c_g are the phase- and group-velocities, respectively.

For a wavenumber ξ_n ($n = 1, 2, \cdots, N$), the angular frequency ω_{mn} ($m = 1, 2, \cdots, M$) that satisfied the dispersion equation $f(\omega_{mn}, \xi_n) = 0$ was determined using the bisection method. The criterion for the determination was that $\Delta\omega$ should be small enough to avoid the omission of roots. However, if $\Delta\omega$ is too small, the computation will be time-consuming. To improve the computation efficiency and avoid the omission of roots, an adaptive bisection scheme was used in this study. The scheme is summarized as follows:

i) For the first wavenumber ξ_1, a fixed searching step is used to find M roots of $f(\omega, \xi_1) = 0$, which are denoted as ω_{m1} (m = 1, 2, …,

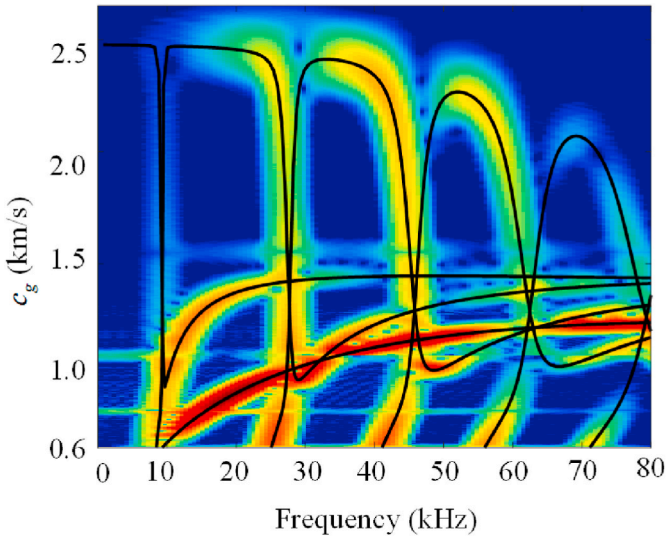

Fig. 4. Frequency-group velocity distribution corresponding to the received transient waveform and the group-velocity dispersion curves obtained by solving the dispersion equation.

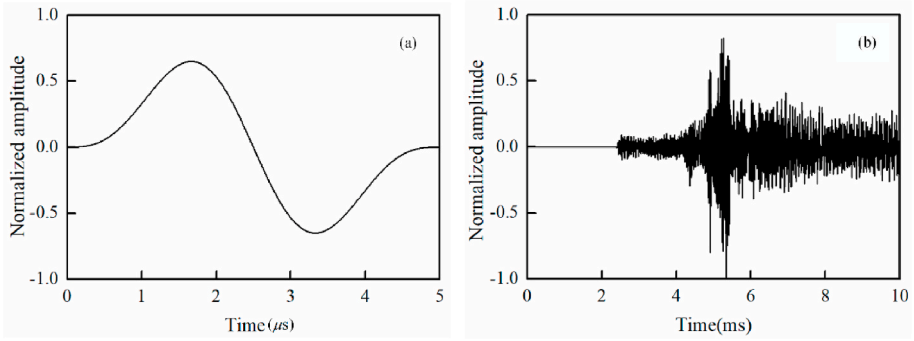

Fig. 3. Time waveform of the applied external force (a) and normal displacement at the receiving point R (b).

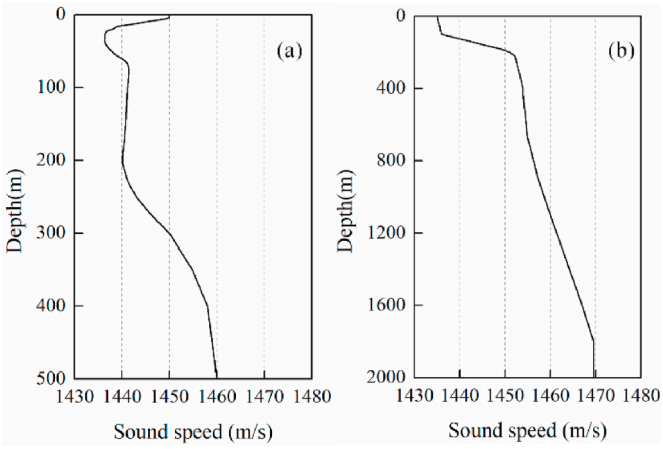

Fig. 5. Sound speed profiles in the Arctic Ocean at depths of (a) 500 m (Li et al., 2014) and (b) 2000 m (Hope et al., 2017).

M). The intervals between adjacent roots are denoted as $\Delta\omega_{m1}$ ($m = 1, 2, \ldots, M\text{-}1$).

ii) For the second wavenumber ξ_2, the step size is adjusted according to ω_{m1} and $\Delta\omega_{m1}$. For example, the step size is set as $\Delta\omega_{m1}/l$ when ω approaches ω_{m1}, where l is a constant. M roots satisfying $f(\omega, \xi_2) = 0$ are denoted as ω_{m2} and the intervals between the adjacent roots are denoted as $\Delta\omega_{m2}$ ($m = 1, 2, \ldots, M\text{-}1$).

iii) Similarly, for the wavenumber ξ_n ($n = 3, 4, \cdots, N$), the step size is adjusted according to $\omega_{m(n-1)}$ and $\Delta\omega_{m(n-1)}$ corresponding to the wavenumber ξ_{n-1}.

4.2. Verification of codes

The reliability of the calculation codes developed in this study was verified. The verification procedure is as follows:

(1) Transient waves in the ice–seawater–sediment system were simulated using the finite element method (FEM). A small three-layered structure, as shown in Fig. 2, was used as an example. The densities of ice, seawater, and sediment were 1000 (Li et al., 2014), 1000, and 1600 kg/m^3 (Li et al., 2014), respectively. The thicknesses of ice, seawater, and sediment were 0.004, 0.04, and 0.008 m, respectively. Seawater was composed of two layers with equal thicknesses. The radius of the three-layered structure was 20 m. An external force F was applied at the origin O, and the receiving point R was located on the upper surface of the ice, as shown in Fig. 2. The distance between the exciting and receiving points was 6 m. Axisymmetric elements with a mesh size of 0.4 mm × 0.4 mm were used in the simulation. The external force was a windowed single sine pulse signal with a center frequency of 200 kHz, as shown in Fig. 3(a). The velocities corresponding to the longitudinal and transverse waves in ice were 3000 and 1400 m/s, respectively (Li et al., 2014). The sound speeds at the upper and lower seawater layers were 1440 and 1470 m/s, respectively. The sound speed at the sediment was 1580 m/s (Li et al., 2014). Fig. 3(b) shows the received waveform of the transient normal displacement.

(2) The time-frequency distribution of the received waveform was obtained using the short-time Fourier transform (STFT). The time axis in the time-frequency distribution was converted into group velocity as the time reflects the speed of wave propagation.

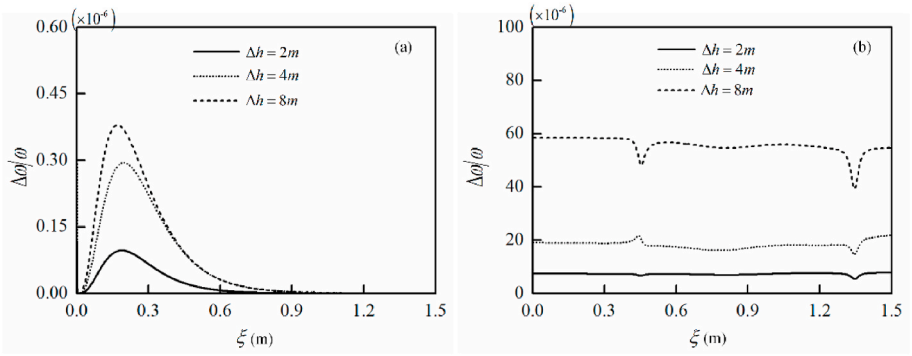

Fig. 6. Relative error of the numerical results for $\Delta h_2 = 1$ m and those for $\Delta h_2 = 2$, 4, and 8 m when solving the dispersion equation for waves propagating at a 500 m-depth of the Arctic Ocean shown in Fig. 5(a) with ice cover: (a) first mode and (b) 100th mode.

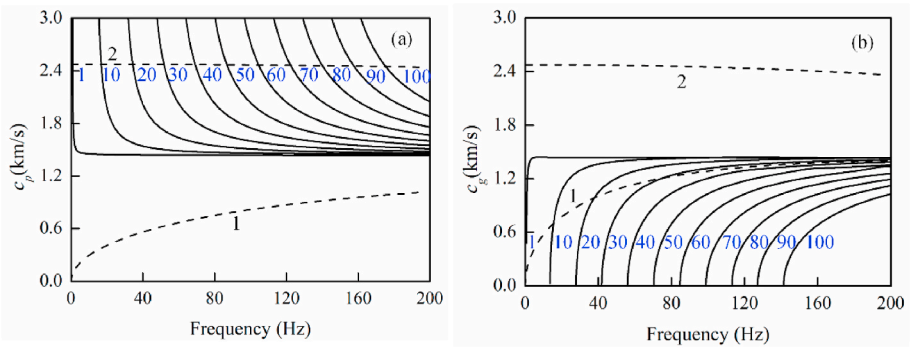

Fig. 7. Dispersion curves for waves propagating at a 500 m-depth of the Arctic Ocean, shown in Fig. 5(a), without ice cover (solid lines) and in a 2 m-thick free ice cover (dotted lines): (a) phase-velocity curves and (b) group-velocity curves.

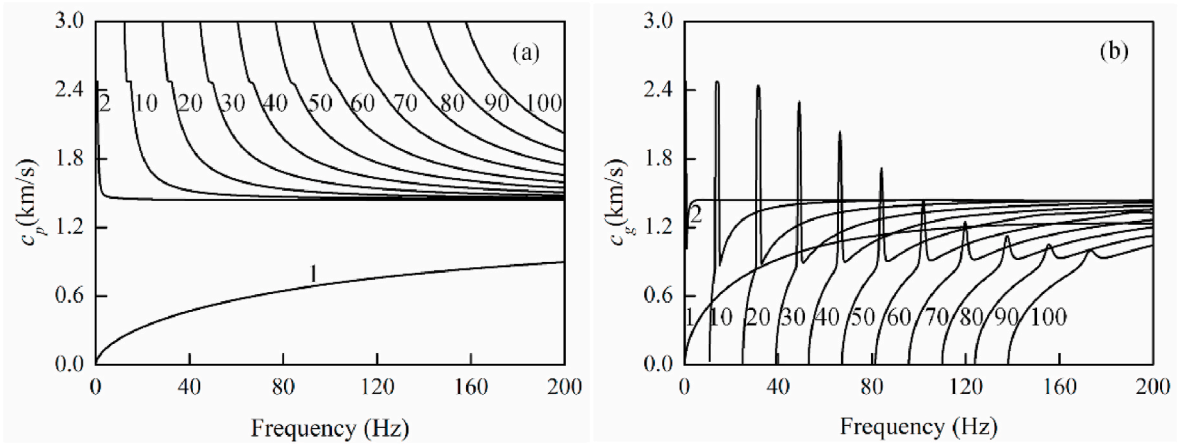

Fig. 8. Dispersion curves for waves propagating at 500 m-depth of the Arctic Ocean shown in Fig. 5(a) with a 2 m-thick ice-cover; (a) phase-velocity curves and (b) group-velocity curves.

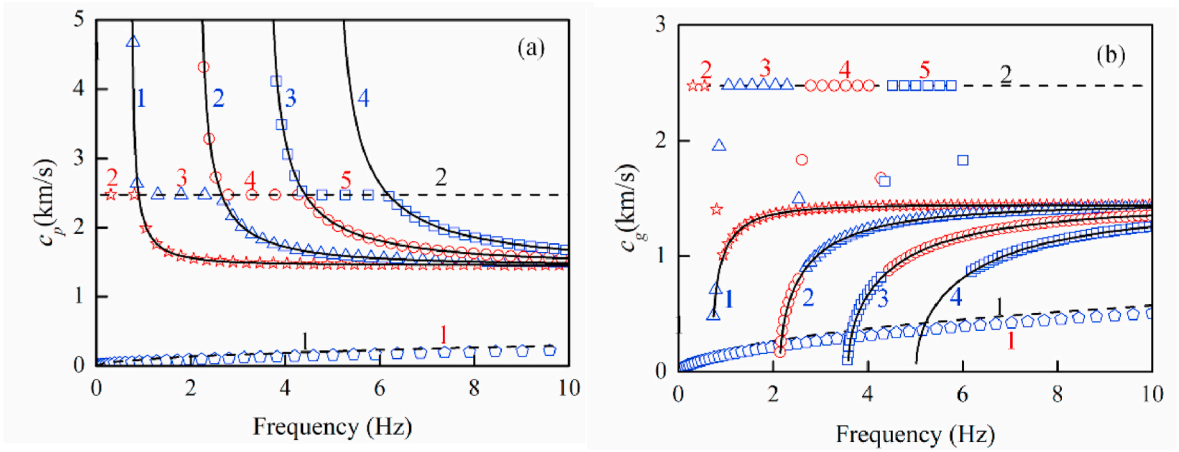

Fig. 9. Dispersion curves of the first several modes for waves propagating at a 500 m-depth of the Arctic Ocean, shown in Fig. 5(a), with (scatters) and without (lines) ice cover, and in a 2 m-thick free ice layer (dotted lines): (a) phase-velocity curves and (b) group-velocity curves.

Consequently, a frequency-group velocity distribution—the group-velocity dispersion diagram, was obtained.

(3) The theoretical derivation and the codes developed to solve the dispersion equation were assumed correct if the group-velocity dispersion curves obtained from solving the dispersion equation agree well with the frequency-group velocity distribution of the transient waves calculated using FEM.

The cloud picture, shown in Fig. 4, is the frequency–group distribution for the transient waveform, shown in Fig. 3(b). The black lines in Fig. 4 are the group-velocity dispersion curves obtained by solving the dispersion equation. Their good agreement indicates that both the theoretical derivation and the codes developed to solve the dispersion equation are correct.

4.3. Numerical results and discussions

The parameters used in this portion of the study are as follows: the thicknesses of the ice cover were 2, 4, 6 and 8 m, the thickness of the sediment were 10 m, and the depths of seawater considered were 500 and 2000 m, respectively. The sound speed profiles at these depths are shown in Fig. 5. The other parameters were the same as those in Section 4.2. It is noted that the ice cover was assumed homogeneous, and Δh_1 was set at h_1 for the purpose of simplifying analysis here.

The selection of Δh_2 influences the calculation accuracy. Theoretically, the smaller the Δh_2, the higher the calculation accuracy. However, the calculation will be time-consuming if Δh_2 is too small. The numerical results for $\Delta h_2 = 1$ m were used as a reference. Fig. 6 shows the relative error between the reference and the results for $\Delta h_2 = 2$, 4, and 8 m at the 500 m-depth Arctic Ocean with ice cover. Fig. 6(a) and (b) present the results for the first and 100th modes, respectively. The higher the Δh, the greater the relative error, as shown in Fig. 6; however, the relative error for $\Delta h_2 = 8$ m was relatively small. The relative errors for the first and 100th modes were less than 0.38×10^{-6} and 8.43×10^{-6}, respectively, when ξ was less than 1.5 m. Note that the results for the high-order modes were more sensitive to the variation in Δh_2 than those for the low-order modes. To minimize the computation time and ensure computation accuracy, Δh_2 was set at 2 m in the calculations.

The solid lines in Fig. 7(a) and (b) are the phase- and group-velocity dispersion curves, respectively, for waves propagating at a 500 m-depth ocean, shown in Fig. 5(a), without ice cover. The dotted lines in Fig. 7(a) and (b) are the phase- and group-velocity dispersion curves, respectively, for waves propagating at a 2 m-thick free ice cover. Fig. 8(a) and (b) show the phase- and group-velocity dispersion curves, respectively, for waves propagating at a 500 m-depth, shown in Fig. 5(a), with a 2 m-thick ice cover.

Comparing Figs. 7 and 8 reveals that the dispersion curves for the waves propagating in the Arctic Ocean with ice cover have significant differences from those without ice cover. The first difference is that a new mode, i.e., the first mode appears for the Arctic Ocean with ice

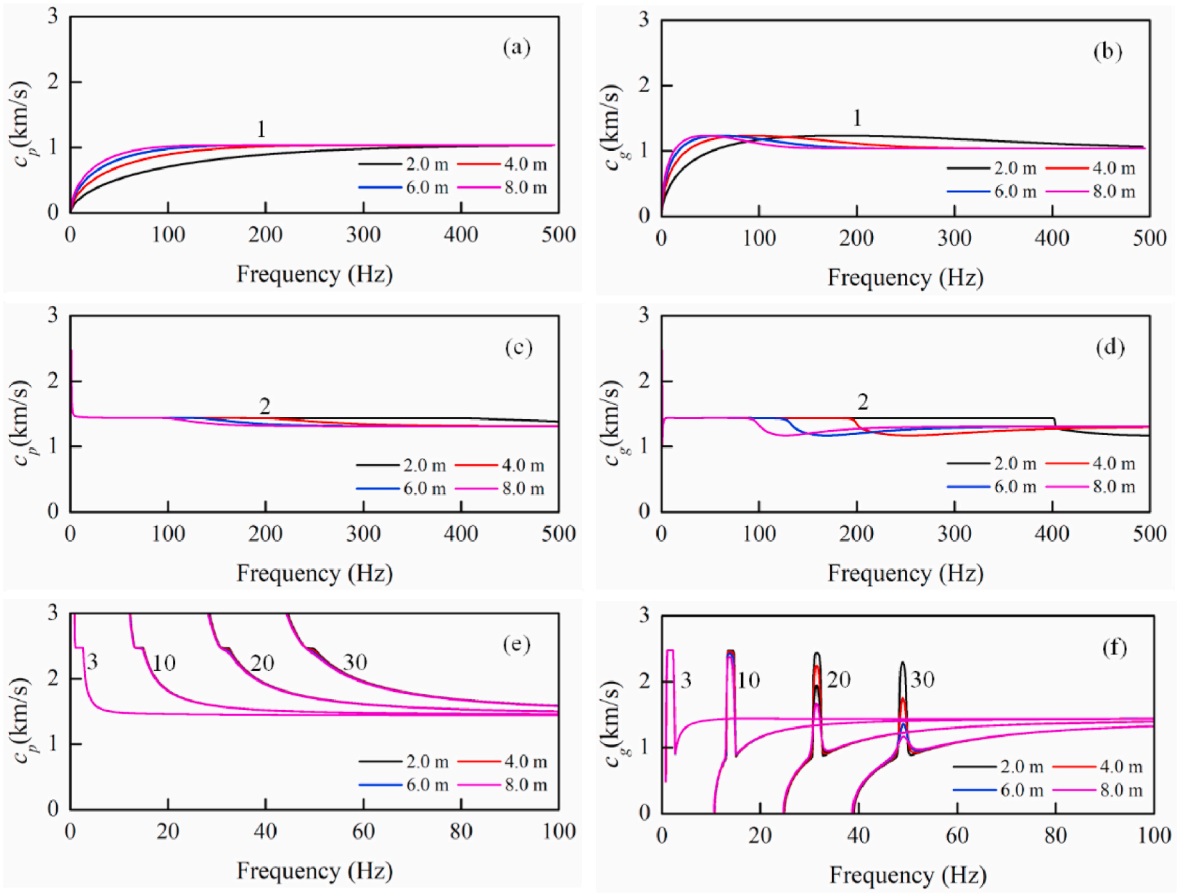

Fig. 10. Dispersion curves for waves propagating at 500 m-depth of the Arctic Ocean shown in Fig. 5(a) with ice cover of different thicknesses: (a) phase-velocity curves and (b) group-velocity curves.

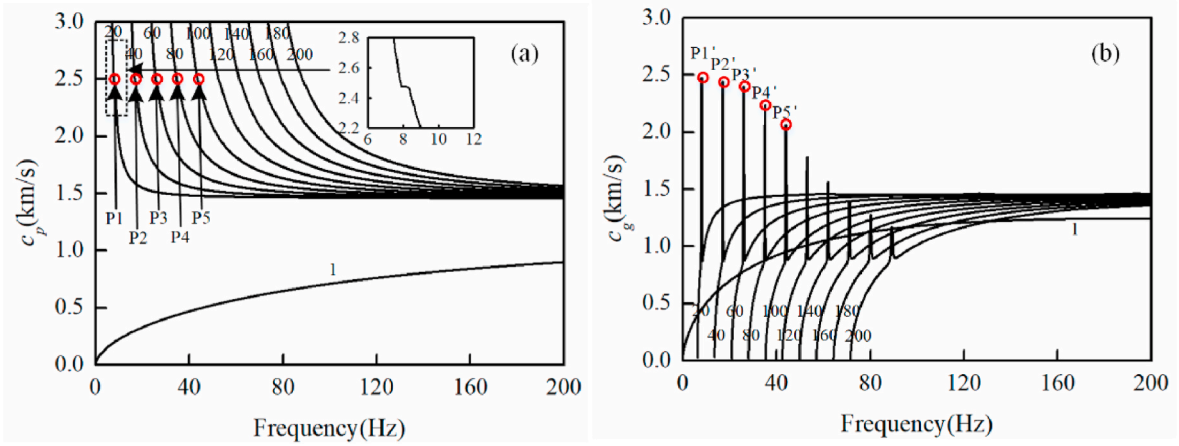

Fig. 11. Dispersion curves for waves propagating at a 2000 m-depth, shown in Fig. 5(b), with a 2 m-thick ice cover: (a) phase-velocity curves and (b) group-velocity curves.

cover. The phase-velocity of the first mode increases initially with an increase in frequency and approaches a stable value as the frequency becomes extremely large, whereas the group-velocity of the first mode increases initially, then slightly decreases, and finally increases with an increase in frequency. It approaches a stable value as the frequency becomes extremely large. The second difference is that the phase-velocity curves for all modes except the first have a slight distortion for the Arctic Ocean with ice cover. The slight distortion in the phase-velocity curve caused a drastic change in the corresponding group-velocity, which results in several sharp peaks, as shown in Fig. 8(b). The peak value of the second mode was at its maximum and decreased with an increase in the mode order.

The dispersion curves for the Arctic Ocean with ice cover were found to be formed by coupling those without ice cover and those in the ice cover through further analyzing the dispersion curves. As shown in Fig. 9, the first mode arises from the first mode in the ice cover, the second mode is formed by coupling a portion of the second mode in the ice cover and the latter portion of the first mode in the Arctic Ocean

without ice cover. The third mode is formed by coupling the former portion of the first mode in the Arctic Ocean without ice cover, a portion of the second mode in the ice cover, and the latter portion of the second mode in the Arctic Ocean without ice cover. Similarly, the n-th ($n > 3$) mode is formed by coupling the former portion of the (n-2)-th mode in the Arctic Ocean without ice cover, a portion of the second mode in the ice cover, and the latter portion of the (n-1)-th mode in the Arctic Ocean without ice cover.

Fig. 10 shows that the variation of the ice cover thickness has a great influence on the dispersion curves of the first and second modes in the Arctic Ocean. For instance, the phase-velocity curve of the first mode increases faster and approaches a stable value at a lower frequency as the ice cover thickness increases. The group-velocity of the second mode decreases initially and then increases gradually with an increase in frequency after exceeding a specific value of 393 Hz for a 2 m-thick ice cover. The thicker the ice cover, the smaller the specific value of the frequency is. In the calculated frequency range (0–500 Hz), the change in the ice cover thickness has little influence on the dispersion curves of the n-th ($3 \le n < 10$) modes; however, it influences those of the n-th ($n \ge 10$) modes to a certain extent. As shown in Fig. 10(f), the peak values of the group-velocity for the 10th, 20th, and 30th modes decrease with an increase in the ice cover thickness; however, the frequencies corresponding to the peak values remain unchanged.

Fig. 11(a) and (b) show the phase- and group-velocity dispersion curves, respectively, for waves propagating at a 2000 m-depth, shown in Fig. 5(b), with a 2m-thick ice cover. Comparing Figs. 11 and 8 reveals that the dispersion curves significantly depend on the seawater depth. The deeper the seawater, the denser are the dispersion curves, and the richer is the guided waves in the same frequency range. However, the coupling mechanism between the seawater and ice cover is the same for both deep and shallow Arctic Ocean.

5. Conclusions

The transfer matrixes corresponding to thin ice and seawater layers were derived. Based on this, a dispersion equation for the waves propagating in the ice-covered Arctic Ocean was derived. The dispersion of waves propagating at depths of 500 and 2000 m were numerically investigated. The results show that the dispersion curves for the Arctic with ice cover are significantly more complex than those without ice cover.

The first mode resulted from the first mode in the ice cover. The second mode was formed by coupling a portion of the second mode in the ice cover and the latter portion of the first mode in the Arctic Ocean without ice cover, whereas the n-th ($n \ge 3$) mode is formed by coupling the former portion of the (n-2)-th mode in the Arctic Ocean without ice cover, a portion of the second mode in the ice cover, and the latter portion of the (n-1)-th mode in the Arctic Ocean without ice cover. The phase-velocity curve for the n-th ($n > 2$) mode exhibited a slight distortion, which caused a sharp peak in the group-velocity curve owning to the coupling effect.

The variation of the ice cover thickness had a significant influence on the dispersion curves of the first and second modes and considerable influence on those of the n-th ($n \ge 10$) mode, whereas it has little influence on those of the n-th ($3 \le n < 10$) mode. Seawater depth is another factor affecting the dispersion curves: the deeper the seawater, the denser the dispersion curves, and the richer the guided waves in the same frequency range.

The transfer matrix technique developed in this study can be generalized to the ice-covered Arctic Ocean with other kinds of sediment modeling, such as elastic solid seafloor, in which both longitudinal and transverse waves are required to investigate the dynamics. Furthermore, the theoretical and numerical results obtained in this study are useful for interpreting the acoustic experimental results in the Arctic Ocean.

Appendix A. Elements of transfer matrix $\mathbf{M}_{1,i}$ (i=1, 2, …, n_1)

$$(M_{1,i})_{11} = \frac{\cos(\alpha_{1,i}\Delta h_1)\left(\beta_{1,i}^2 - \xi^2\right) + 2\xi^2\cos(\beta_{1,i}\Delta h_1)}{\left(\xi^2 + \beta_{1,i}^2\right)}$$

$$(M_{1,i})_{12} = \frac{\xi}{\left(\xi^2 + \beta_{1,i}^2\right)}\left[-2\alpha_{1,i}\sin(\alpha_{1,i}\Delta h_1) + \frac{\left(\beta_{1,i}^2 - \xi^2\right)\sin(\beta_{1,i}\Delta h_1)}{\beta_{1,i}}\right]\frac{J_0(\xi r)}{J_0'(\xi r)}$$

$$(M_{1,i})_{13} = \frac{1}{\mu_{1,i}\left(\xi^2 + \beta_{1,i}^2\right)}\left[\alpha_{1,i}\sin(\alpha_{1,i}\Delta h_1) + \frac{\xi^2\sin(\beta_{1,i}\Delta h_1)}{\beta_{1,i}}\right]$$

$$(M_{1,i})_{14} = \frac{\xi}{\mu_{1,i}\left(\xi^2 + \beta_{1,i}^2\right)}\left[\cos(\alpha_{1,i}\Delta h_1) - \cos(\beta_{1,i}\Delta h_1)\right]\frac{J_0(\xi r)}{J_0'(\xi r)}$$

CRediT authorship contribution statement

Shengxing Liu: Writing – review & editing, Supervision, Methodology, Funding acquisition, Conceptualization. **Qitian Zeng:** Writing – original draft, Investigation, Data curation. **Liguo Tang:** Writing – review & editing, Methodology, Conceptualization. **Zhenglin Li:** Writing – review & editing, Methodology, Funding acquisition, Conceptualization.

Declaration of competing interest

The authors declare that they have no known competing financial interests or personal relationships that could have appeared to influence the work reported in this paper.

Data availability

Data will be made available on request.

Acknowledgments

This work was supported by the National Natural Science Foundation of China (U22A2012) and the State Key Laboratory of Acoustics, Chinese Academy of Sciences (SKLA202101).

$$(M_{1,i})_{21}=\frac{\xi}{\left(\xi^2+\beta_{1,i}^2\right)}\left[\frac{\left(\beta_{1,i}^2-\xi^2\right)\sin(\alpha_{1,i}\Delta h_1)}{\alpha_{1,i}}-2\beta_{1,i}\sin(\beta_{1,i}\Delta h_1)\right]\frac{J_0^{'}(\xi r)}{J_0(\xi r)}$$

$$(M_{1,i})_{22}=\frac{1}{\left(\xi^2+\beta_{1,i}^2\right)}\left[2\xi^2\cos(\alpha_{1,i}\Delta h_1)+\left(\beta_{1,i}^2-\xi^2\right)\cos(\beta_{1,i}\Delta h_1)\right]$$

$$(M_{1,i})_{23}=\frac{\xi}{\mu_{1,i}\left(\xi^2+\beta_{1,i}^2\right)}\left[-\cos(\alpha_{1,i}\Delta h_1)+\cos(\beta_{1,i}\Delta h_1)\right]\frac{J_0^{'}(\xi r)}{J_0(\xi r)}$$

$$(M_{1,i})_{24}=\frac{1}{\mu_{1,i}\left(\xi^2+\beta_{1,i}^2\right)}\left[\frac{\xi^2\sin(\alpha_{1,i}\Delta h_1)}{\alpha_{1,i}}+\beta_{1,i}\sin(\beta_{1,i}\Delta h_1)\right]$$

$$(M_{1,i})_{31}=\frac{\mu_{1,i}}{\left(\xi^2+\beta_{1,i}^2\right)}\left[-\frac{\left(\beta_{1,i}^2-\xi^2\right)^2\sin(\alpha_{1,i}\Delta h_1)}{\alpha_{1,i}}-4\xi^2\beta_{1,i}\sin(\beta_{1,i}\Delta h_1)\right]$$

$$(M_{1,i})_{32}=\frac{2\mu_{1,i}\xi\left(\xi^2-\beta_{1,i}^2\right)}{\left(\xi^2+\beta_{1,i}^2\right)}\left[\cos(\alpha_{1,i}\Delta h_1)-\cos(\beta_{1,i}\Delta h_1)\right]\frac{J_0(\xi r)}{J_0^{'}(\xi r)}$$

$$(M_{1,i})_{33}=\frac{1}{\left(\xi^2+\beta_{1,i}^2\right)}\left[\left(\beta_{1,i}^2-\xi^2\right)\sin(\alpha_{1,i}\Delta h_1)+2\xi^2\cos(\beta_{1,i}\Delta h_1)\right]$$

$$(M_{1,i})_{34}=\frac{\xi}{\left(\xi^2+\beta_{1,i}^2\right)}\left[\frac{\left(\xi^2-\beta_{1,i}^2\right)\sin(\alpha_{1,i}\Delta h_1)}{\alpha_{1,i}}+2\beta_{1,i}\sin(\beta_{1,i}\Delta h_1)\right]\frac{J_0(\xi r)}{J_0^{'}(\xi r)}$$

$$(M_{1,i})_{41}=\frac{2\mu_{1,i}\xi\left(\beta_{1,i}^2-\xi^2\right)}{\left(\xi^2+\beta_{1,i}^2\right)}\left[\cos(\alpha_{1,i}\Delta h_1)-\cos(\beta_{1,i}\Delta h_1)\right]\frac{J_0^{'}(\xi r)}{J_0(\xi r)}$$

$$(M_{1,i})_{42}=-\frac{\mu_{1,i}}{\left(\xi^2+\beta_{1,i}^2\right)}\left[4\xi^2\alpha_{1,i}\sin(\alpha_{1,i}\Delta h_1)+\frac{\left(\beta_{1,i}^2-\xi^2\right)^2\sin(\beta_{1,i}\Delta h_1)}{\beta_{1,i}}\right]$$

$$(M_{1,i})_{43}=\frac{\xi}{\left(\xi^2+\beta_{1,i}^2\right)}\left[2\alpha_{1,i}\sin(\alpha_{1,i}\Delta h_1)+\frac{\left(\xi^2-\beta_{1,i}^2\right)\sin(\beta_{1,i}\Delta h_1)}{\beta_{1,i}}\right]\frac{J_0^{'}(\xi r)}{J_0(\xi r)}$$

$$(M_{1,i})_{44}=\frac{1}{\xi^2+\beta_{1,i}^2}\left[2\xi^2\cos(\alpha_{1,i}h_1)-\left(\xi^2-\beta_{1,i}^2\right)\cos(\beta_{1,i}h_1)\right]$$

Appendix B. : Elements of matrix M

$$M_{11}^{'}=-\mu_{1,1}\left[\beta_{1,1}^2-\xi^2\right]\cos(\alpha_{1,1}h_1)J_0(\xi r)$$

$$M_{12}^{'}=\mu_{1,1}\left[\beta_{1,1}^2\omega^2-\xi^2\right]\sin(\alpha_{1,1}h_1)J_0(\xi r)$$

$$M_{13}^{'}=2\mu_{1,1}\xi^2\beta_{1,1}\sin(\beta_{1,1}h_1)J_0(\xi r)$$

$$M_{14}^{'}=2\mu_{1,1}\xi^2\beta_{1,1}\cos(\beta_{1,1}h_1)J_0(\xi r)$$

$$M_{15}^{'}=M_{16}^{'}=0$$

$$M_{21}^{'}=2\mu_{1,1}\alpha_{1,1}\xi\sin(\alpha_{1,1}h_1)J_0^{'}(\xi r)$$

$$M_{22}^{'}=2\mu_{1,1}\alpha_{1,1}\xi\cos(\alpha_{1,1}h_1)J_0^{'}(\xi r)$$

$$M_{23}^{'}=2\mu_{1,1}\xi\left(\xi^2-\beta_{1,i}^2\right)\cos(\beta_{1,1}h_1)J_0^{'}(\xi r)$$

$$M_{24}^{'} = -2\mu_{1,1}\xi\left(\xi^2-\beta_{1,i}^2\right)\sin\left(\beta_{1,1}h_1\right)J_0^{'}(\xi r)$$

$$M_{25}^{'} = M_{26}^{'} = 0$$

$$M_{31}^{'} = \left[M_{11}^{\mathrm{I}}\alpha_{\mathrm{I},1}\sin(\alpha_{\mathrm{I},1}h_1) - M_{13}^{\mathrm{I}}\mu_{\mathrm{I},1}\left(\beta_{1,i}^2-\xi^2\right)\cos(\alpha_{\mathrm{I},1}h_1)\right]J_0(\xi r) + \xi\left[M_{12}^{\mathrm{I}}\cos(\alpha_{\mathrm{I},1}h_1) + 2M_{14}^{\mathrm{I}}\mu_{\mathrm{I},1}\alpha_{\mathrm{I},1}\sin(\alpha_{\mathrm{I},1}h_1)\right]J_0^{'}(\xi r)$$

$$M_{32}^{'} = \left[M_{11}^{\mathrm{I}}\alpha_{1,1}\cos\left(\alpha_{1,1}h_1\right) + M_{13}^{\mathrm{I}}\mu_{1,1}\left(\beta_{1,1}^2-\xi^2\right)\sin\left(\alpha_{1,1}h_1\right)\right]J_0(\xi r) + \xi\left[-M_{12}^{\mathrm{I}}\sin\left(\alpha_{1,1}h_1\right) + 2M_{14}^{\mathrm{I}}\mu_{1,1}\alpha_{1,1}\cos\left(\alpha_{1,1}h_1\right)\right]J_0^{'}(\xi r)$$

$$M_{33}^{'} = \xi^2\left[M_{11}^{\mathrm{I}}\cos\left(\beta_{1,1}h_1\right) + 2M_{13}^{\mathrm{I}}\mu_{1,1}\beta_{1,1}\sin\left(\beta_{1,1}h_1\right)\right]J_0(\xi r) + \xi\left[M_{12}^{\mathrm{I}}\beta_{1,1}\sin\left(\beta_{1,1}h_1\right) + 2M_{14}^{\mathrm{I}}\mu_{1,1}\left(\xi^2-\beta_{1,1}^2\right)\cos\left(\beta_{1,1}h_1\right)\right]J_0^{'}(\xi r)$$

$$M_{34}^{'} = \xi^2\left[-M_{11}^{\mathrm{I}}\sin\left(\beta_{1,1}h_1\right) + 2M_{13}^{\mathrm{I}}\mu_{1,1}\beta_1^{\mathrm{I}}\cos\left(\beta_1^{\mathrm{I}}h_1\right)\right]J_0(\xi r) + \xi\left[M_{12}^{\mathrm{I}}\beta_{1,1}\cos\left(\beta_{1,1}h_1\right) - 2M_{14}^{\mathrm{I}}\mu_{1,1}\left(\xi^2-\beta_{\mathrm{I},1}^2\right)\sin\left(\beta_{1,1}h_1\right)\right]J_0^{'}(\xi r)$$

$$M_{35}^{'} = 0$$

$$M_{36}^{'} = \alpha_{\mathrm{II},1}J_0(\xi r)$$

$$M_{41}^{'} = \left[M_{31}^{\mathrm{I}}\alpha_{\mathrm{I},1}\sin(\alpha_{\mathrm{I},1}h_1) - M_{33}^{\mathrm{I}}\mu_{\mathrm{I},1}\left(\beta_{1,i}^2-\xi^2\right)\cos(\alpha_{\mathrm{I},1}h_1)\right]J_0(\xi r) + \xi\left[M_{32}^{\mathrm{I}}\cos(\alpha_{\mathrm{I},1}h_1) + 2M_{34}^{\mathrm{I}}\mu_{\mathrm{I},1}\alpha_{\mathrm{I},1}\sin(\alpha_{\mathrm{I},1}h_1)\right]J_0^{'}(\xi r)$$

$$M_{42}^{'} = \left[M_{31}^{\mathrm{I}}\alpha_{1,1}\cos\left(\alpha_{1,1}h_1\right) + M_{33}^{\mathrm{I}}\mu_{1,1}\left(\beta_{1,1}^2-\xi^2\right)\sin\left(\alpha_{1,1}h_1\right)\right]J_0(\xi r) + \xi\left[-M_{32}^{\mathrm{I}}\sin\left(\alpha_{1,1}h_1\right) + 2M_{34}^{\mathrm{I}}\mu_{1,1}\alpha_{1,1}\cos\left(\alpha_{1,1}h_1\right)\right]J_0^{'}(\xi r)$$

$$M_{43}^{'} = \xi^2\left[M_{31}^{\mathrm{I}}\cos\left(\beta_{1,1}h_1\right) + 2M_{33}^{\mathrm{I}}\mu_{1,1}\beta_{1,1}\sin\left(\beta_{1,1}h_1\right)\right]J_0(\xi r) + \xi\left[M_{32}^{\mathrm{I}}\beta_{1,1}\sin\left(\beta_{1,1}h_1\right) + 2M_{34}^{\mathrm{I}}\mu_{1,1}\left(\xi^2-\beta_{1,1}^2\right)\cos\left(\beta_{1,1}h_1\right)\right]J_0^{'}(\xi r)$$

$$M_{44}^{'} = \xi^2\left[-M_{31}^{\mathrm{I}}\sin\left(\beta_{1,1}h_1\right) + 2M_{33}^{\mathrm{I}}\mu_{1,1}\beta_1^{\mathrm{I}}\cos\left(\beta_1^{\mathrm{I}}h_1\right)\right]J_0(\xi r) + \xi\left[M_{32}^{\mathrm{I}}\beta_{1,1}\cos\left(\beta_{1,1}h_1\right) - 2M_{34}^{\mathrm{I}}\mu_{1,1}\left(\xi^2-\beta_{\mathrm{I},1}^2\right)\sin\left(\beta_{1,1}h_1\right)\right]J_0^{'}(\xi r)$$

$$M_{45}^{'} = -\rho_{\mathrm{II},1}\omega^2J_0(\xi r)$$

$$M_{46}^{'} = 0$$

$$M_{51}^{'} = \left[M_{41}^{\mathrm{I}}\alpha_{\mathrm{I},1}\sin(\alpha_{\mathrm{I},1}h_1) - M_{43}^{\mathrm{I}}\mu_{\mathrm{I},1}\left(\beta_{1,i}^2-\xi^2\right)\cos(\alpha_{\mathrm{I},1}h_1)\right]J_0(\xi r) + \xi\left[M_{42}^{\mathrm{I}}\cos(\alpha_{\mathrm{I},1}h_1) + 2M_{44}^{\mathrm{I}}\mu_{\mathrm{I},1}\alpha_{\mathrm{I},1}\sin(\alpha_{\mathrm{I},1}h_1)\right]J_0^{'}(\xi r)$$

$$M_{52}^{'} = \left[M_{41}^{\mathrm{I}}\alpha_{1,1}\cos\left(\alpha_{1,1}h_1\right) + M_{43}^{\mathrm{I}}\mu_{1,1}\left(\beta_{1,1}^2-\xi^2\right)\sin\left(\alpha_{1,1}h_1\right)\right]J_0(\xi r) + \xi\left[-M_{42}^{\mathrm{I}}\sin\left(\alpha_{1,1}h_1\right) + 2M_{44}^{\mathrm{I}}\mu_{1,1}\alpha_{1,1}\cos\left(\alpha_{1,1}h_1\right)\right]J_0^{'}(\xi r)$$

$$M_{53}^{'} = \xi^2\left[M_{41}^{\mathrm{I}}\cos\left(\beta_{1,1}h_1\right) + 2M_{43}^{\mathrm{I}}\mu_{1,1}\beta_{1,1}\sin\left(\beta_{1,1}h_1\right)\right]J_0(\xi r) + \xi\left[M_{42}^{\mathrm{I}}\beta_{1,1}\sin\left(\beta_{1,1}h_1\right) + 2M_{44}^{\mathrm{I}}\mu_{1,1}\left(\xi^2-\beta_{1,1}^2\right)\cos\left(\beta_{1,1}h_1\right)\right]J_0^{'}(\xi r)$$

$$M_{54}^{'} = \xi^2\left[-M_{41}^{\mathrm{I}}\sin\left(\beta_{1,1}h_1\right) + 2M_{43}^{\mathrm{I}}\mu_{1,1}\beta_1^{\mathrm{I}}\cos\left(\beta_1^{\mathrm{I}}h_1\right)\right]J_0(\xi r) + \xi\left[M_{42}^{\mathrm{I}}\beta_{1,1}\cos\left(\beta_{1,1}h_1\right) - 2M_{44}^{\mathrm{I}}\mu_{1,1}\left(\xi^2-\beta_{\mathrm{I},1}^2\right)\sin\left(\beta_{1,1}h_1\right)\right]J_0^{'}(\xi r)$$

$$M_{55}^{'} = M_{56}^{'} = 0$$

$$M_{61}^{'} = M_{62}^{'} = M_{63}^{'} = M_{64}^{'} = 0$$

$$M_{65}^{'} = -M_{12}^{\mathrm{II}}\rho_{\mathrm{II},1}\omega^2J_0(\xi r)$$

$$M_{66}^{'} = M_{11}^{\mathrm{II}}\alpha_{\mathrm{II},1}J_0(\xi r)$$

References

Boyles, C.A., 1983. Coupled mode solution for a cylindrically symmetric oceanic waveguide with a range and depth dependent refractive index and a time varying rough sea surface. J. Acoust. Soc. Am. 73 (3), 800–805.

Burke, J.E., Twersky, V., 1966. Scattering and reflection by elliptically striated surfaces. J. Acoust. Soc. Am. 40 (4), 883–895.

Collis, J.M., Frank, S.D., Metzler, A.M., Preston, K.S., 2016. Elastic parabolic equation and normal mode solutions for seismo-acoustic propagation in underwater environments with ice covers. J. Acoust. Soc. Am. 139 (5), 2672–2682.

Diachok, O.I., 1976. Effects of sea-ice ridges on sound propagation in the Arctic Ocean. J. Acoust. Soc. Am. 59 (5), 1110–1120.

Eringen, A.C., Suhubi, E.S., 1975. Elastodynamics, vol. II. Academic Press, New York.

Frank, S.D., Ivakin, A.N., 2018. Long-range reverberation in an Arctic environment: effects of ice thickness and elasticity. J. Acoust. Soc. Am. 143 (3), EL167–EL173.

Freitag, L., Ball, K., Partan, J., Koski, P., Singh, S., 2015. Long range acoustic communications and navigation in the Arctic. In: OCEANS 2015-MTS/IEEE Washington, pp. 1–5. IEEE.

Gavrilov, A.N., Mikhalevsky, P.N., 2006. Low-frequency acoustic propagation loss in the Arctic Ocean: results of the Arctic climate observations using underwater sound experiment. J. Acoust. Soc. Am. 119 (6), 3694–3706.

Haas, C., Hendricks, S., Eicken, H., Herber, A., 2010. Synoptic airborne thickness surveys reveal state of Arctic sea ice cover. Geophys. Res. Lett. 37 (9).

He, T., Wang, B., Tang, S., Zhou, F., Mo, S., Fang, E., 2023. Numerical simulation of wave propagation in ice-covered ocean environments based on the equivalent-source method. Phys. Fluids 35 (4).

Hope, G., Sagen, H., Storheim, E., Hobæk, H., Freitag, L., 2017. Measured and modeled acoustic propagation underneath the rough Arctic sea-ice. J. Acoust. Soc. Am. 142 (3), 1619–1633.

Hunkins, K., Kutschale, H., 1963. Shallow-water propagation in the Arctic Ocean. J. Acoust. Soc. Am. 35 (4), 542–551.

Jensen, F.B., Kuperman, W.A., Porter, M.B., Schmidt, H., 2011. Computational Ocean Acoustics. Springer New York, New York, NY, p. 38.

Jezek, K.C., Stanton, T.K., Gow, A.J., Lange, M.A., 1990. Influence of environmental conditions on acoustical properties of sea ice. J. Acoust. Soc. Am. 88 (4), 1903–1912.

Keen, K.A., Thayre, B.J., Hildebrand, J.A., Wiggins, S.M., 2018. Seismic airgun sound propagation in Arctic Ocean waveguides. Deep-Sea Res. PT. I 141, 24–32.

Kutschale, H., 1961. Long-range sound transmission in the Arctic Ocean. J. Geophys. Res. 66 (7), 2189–2198.
Kwok, R., Rothrock, D.A., 2009. Decline in Arctic sea ice thickness from submarine and ICESat records: 1958–2008. Geophys. Res. Lett. 36 (15).
LePage, K., Schmidt, H., 1994. Modeling of low-frequency transmission loss in the central Arctic. J. Acoust. Soc. Am. 96 (3), 1783–1795.
Li, Q., Wang, N., Zhao, J., et al., 2014. Arctic underwater acoustics: an attractive new topic in ocean acoustics. J. Appl. Acoust. 33 (6), 471–483.
Liu, S., Song, A., Shen, C.C., 2019. Topology Optimization of long-thin sensor Networks in under-ice environments. IEEE J. Oceanic Eng. 44 (4), 1264–1278.
McCammon, D.F., McDaniel, S.T., 1985. The influence of the physical properties of ice on reflectivity. J. Acoust. Soc. Am. 77 (2), 499–507.
Mikhalevsky, P.N., Gavrilov, A.N., Baggeroer, A.B., 1999. The transarctic acoustic propagation experiment and climate monitoring in the Arctic. IEEE J. Oceanic Eng. 24 (2), 183–201.
Münchow, A., Padman, L., Fricker, H.A., 2014. Interannual changes of the floating ice shelf of Petermann Gletscher, North Greenland, from 2000 to 2012. J. Glaciol. 60 (221), 489–499.
Penhale, M.B., Barnard, A.R., Shuchman, R., 2018. Multi-modal and short-range transmission loss in thin, ice-covered, near-shore Arctic waters. J. Acoust. Soc. Am. 143 (5), 3126–3137.
Porter, M.B., Reiss, E.L., 1984. A numerical method for ocean-acoustic normal modes. J. Acoust. Soc. Am. 76 (1), 244–252.
Porter, M.B., Reiss, E.L., 1985. A numerical method for bottom interacting ocean acoustic normal modes. J. Acoust. Soc. Am. 77 (5), 1760–1767.
Schwarz, J., Weeks, W.F., 1977. Engineering properties of sea ice. J. Glaciol. 19 (81), 499–531.
Shroyer, E.L., Padman, L., Samelson, R.M., Münchow, A., Stearns, L.A., 2017. Seasonal control of Petermann Gletscher ice-shelf melt by the ocean's response to sea-ice cover in Nares Strait. J. Glaciol. 63 (238), 324–330.